

The Column Density Distribution Function at $z = 0$ from H_I Selected Galaxies.

Emma V. Ryan-Weber,^{1,2} Rachel L. Webster¹ and Lister Staveley-Smith²

¹*School of Physics, Univeristy of Melbourne, VIC 3010 Australia*

²*Australia Telescope National Facility, CSIRO, PO Box 76, Epping, NSW 1710, Australia*

Accepted ***. Received ***; in original form ***

ABSTRACT

We have measured the column density distribution function, $f(N_{\text{HI}})$, at $z = 0$ using 21-cm HI emission from galaxies selected from a blind HI survey. $f(N_{\text{HI}})$ is found to be smaller and flatter at $z = 0$ than indicated by high-redshift measurements of Damped Lyman- α (DLA) systems, consistent with the predictions of hierarchical galaxy formation. The derived DLA number density per unit redshift, $dN_{\text{DLA}}/dz = 0.058$, is in moderate agreement with values calculated from low-redshift QSO absorption line studies. We use two different methods to determine the types of galaxies which contribute most to the DLA cross-section: comparing the power law slope of $f(N_{\text{HI}})$ to theoretical predictions and analysing contributions to dN_{DLA}/dz . We find that comparison of the power law slope cannot rule out spiral discs as the dominant galaxy type responsible for DLA systems. Analysis of dN_{DLA}/dz however, is much more discriminating. We find that galaxies with $\log M_{\text{HI}} < 9.0$ make up 34% of dN_{DLA}/dz ; Irregular and Magellanic types contribute 25%; galaxies with surface brightness, $\bar{\mu}_{25} > 24$ mag arcsec⁻² account for 22% and sub- L_* galaxies contribute 45% to dN_{DLA}/dz . We conclude that a large range of galaxy types give rise to DLA systems, not just large spiral galaxies as previously speculated.

Key words: galaxies: ISM, quasars: absorption lines

1 INTRODUCTION

Lyman- α ($\text{Ly}\alpha$) absorption systems, in the continuum spectra of background QSOs, provide a powerful probe of the distribution of neutral hydrogen in the Universe. Damped $\text{Ly}\alpha$ (DLA) systems have column densities $N_{\text{HI}} \geq 2 \times 10^{20} \text{cm}^{-2}$ and contain the bulk of the neutral gas in the Universe (Storrie-Lombardi & Wolfe 2000). The value of Ω_{gas} from DLAs at high redshift agrees well with Ω_{star} in present day galaxies. The fact that Ω_{gas} decreases monotonically with decreasing redshift and approaches $\Omega_{\text{gas}}(z = 0)$ from 21-cm emission of local galaxies also provides strong evidence that DLAs are caused by galaxies (Wolfe et al. 1995). The properties of these galaxies however, remain mostly unconstrained.

There are two primary competing theories on the evolution of neutral gas in galaxies. The first is monolithic collapse of protogalactic discs (Wolfe et al. 1986). This scenario, supported by Prochaska & Wolfe (1997), proposes that the kinematics of neutral gas tracing-ions in DLAs are best described by thick, rotating galactic discs. Alternatively, neutral gas in galaxies could be accreted hierarchically from sub-galactic halos. Haehnelt et al. (1998) argue

that the kinematics of DLAs can equally be explained by sight-lines through irregular protogalactic clumps.

Since massive spiral galaxies contain the bulk of the HI at $z = 0$, it has been presumed that they also account for most of the $N_{\text{HI}} \geq 2 \times 10^{20} \text{cm}^{-2}$ cross-section (e.g. Wolfe et al. 1986; Rao & Briggs 1993). With the advent of space-based UV spectroscopy, and the discovery of low redshift ($z < 1.65$) DLAs, this assumption can now be tested. At low redshift the galaxies responsible for DLAs can be resolved, so their luminosities, surface brightness and morphological types can be determined.

At $z < 1.65$ fewer than 30 DLAs are known. Images of 15 DLA galaxies have been published. The morphological breakdown includes 7 low surface brightness (LSB) galaxies, 6 spirals and 2 compact dwarf-like galaxies (Le Brun et al. 1997; Pettini et al. 2000; Turnshek et al. 2001; Bowen et al. 2001; Nestor et al. 2002). These galaxies are distributed evenly in luminosity, with 7 galaxies having $L < L_*$. Only five of these galaxies have measured spectroscopic redshifts. Unless the galaxy has a confirmed redshift matching that of the absorption systems, it is not certain that a particular galaxy is responsible for a DLA system.

To determine the HI emission properties of these DLA galaxies, they need to have even lower redshifts

(due to the weakness of the 21-cm transition). There is only one case of HI emission detected from a DLA galaxy. The DLA galaxy SBS 1543+593 (Bowen et al. 2001) has been detected (Bowen et al. 2001) and mapped (Chengalur & Kanekar 2002) in 21-cm. The candidate ($\text{Ly}\alpha$ column density yet to be published) DLA galaxy NGC 4203 reported by Miller et al. (1999) has also been mapped in 21-cm (van Driel et al. 1988).

For a set of random QSO sight-lines, DLA absorbers simply map out the cross-section on the sky with $N_{\text{HI}} \geq 2 \times 10^{20} \text{ cm}^{-2}$. For this reason, it is not surprising to find a variety of galaxies responsible for DLAs. There are also theoretical suggestions that different galaxy types, such as LSB galaxies may contribute significantly to the high N_{HI} cross-section (Jimenez et al. 1999; Boissier et al. 2002). One way to characterize this cross-section is to use the column density distribution function, $f(N_{\text{HI}})$.

$f(N_{\text{HI}})$ is defined as the number of absorbers in the range N_{HI} to $N_{\text{HI}} + dN_{\text{HI}}$ per unit N_{HI} per unit absorption distance. The most recent determination of $f(N_{\text{HI}})$ over a range of redshifts, using a statistical sample of 646 QSOs, with 85 measured DLAs, is by Storrie-Lombardi & Wolfe (2000). At low redshift, DLAs are rare due to the low volume of space surveyed by QSO sight-lines and the fact the spectral observations must be made in the UV. To increase the number statistics, Rao & Turnshek (2000) used an alternative approach by selecting candidate DLAs from a sample of MgII absorption line systems. Although $\lesssim 30$ DLAs are now known at $z < 1.65$, the number at $z < 0.1$ is still only two. Significant evolution of galaxies (and hence DLAs) is still expected in the range $0 < z < 1.65$. Therefore DLAs are unlikely to provide a suitable technique for measuring $f(N_{\text{HI}})$ at $z = 0$.

Fortunately, at $z = 0$ the alternative method of 21-cm emission can be used to measure $f(N_{\text{HI}})$. The 21-cm emission method has two main advantages. Unlike QSO absorption observations, 21-cm emission does not suffer from the low number statistics. Secondly, since the properties of galaxies detected in 21-cm are known, they can be used to infer the distribution of DLA galaxy properties such as luminosity, surface brightness, and HI mass. Hence we are able to assign the probability that a particular galaxy type gives rise to a DLA at $z = 0$.

Previous calculations of the column density distribution function from 21-cm emission have been published by Rao & Briggs (1993) and Zwaan et al. (1999, 2002). The study by Rao & Briggs (1993) used Arecibo observations of 27 large spiral galaxies. Zwaan et al. (1999, 2002) used synthesis observations of optically-selected Ursa Major cluster members and improved significantly on the previous calculation. The benefit of using a galaxy cluster is that the spatial resolution is the same for each galaxy. However, galaxy clusters are known to be HI-deficient (e.g. Solanes et al. 2001) and may also have flatter HI mass functions (e.g. Rosenberg & Schneider 2002) which could bias the $f(N_{\text{HI}})$ calculation.

To calculate $f(N_{\text{HI}})$ from 21-cm emission we must be confident that 21-cm measurements of N_{HI} are equivalent to those from $\text{Ly}\alpha$ absorption. According to Dickey & Lockman (1990) “The agreement between ultraviolet and radio estimates of N_{HI} is excellent and somewhat astonishing, considering that the angular resolution, experi-

mental techniques, and telescopes differ in all respects”. This statement refers to a comparison of high latitude Galactic 21-cm measurements compared with $\text{Ly}\alpha$ absorption toward distant stars (in the same direction) in the range $10^{20} \leq N_{\text{HI}} \leq 10^{21} \text{ cm}^{-2}$. A further issue is that high column density gas may clump on scales less than the beam size. This concern has been addressed by Rao & Briggs (1993) in their calculation of the contribution of high N_{HI} gas to the HI mass function (which is not affected by beam size) compared with the integral of mass from the $f(N_{\text{HI}})$ cross-section. They find the integral of mass in $f(N_{\text{HI}})$ is equivalent to that from the mass function at high N_{HI} . They concluded that any high N_{HI} column density gas missed due to a large beam size is negligible.

In this paper we calculate $f(N_{\text{HI}})$ from a randomly selected HI sample of galaxies selected from the whole southern sky. This selection process most closely mimics that of random QSO sight-lines. The selection process and observations are described in §2. In §3 $f(N_{\text{HI}})$ at $z = 0$ is calculated and compared to higher redshift measurements. The data set is in then sorted by galaxy properties and the contribution to the cross-section of HI gas satisfying the DLA criterion is calculated. In §4 the implications of the results are discussed and conclusions are presented in §5. Details of the galaxy sample, including HI contour maps and column density histograms are given in the appendix.

2 OBSERVATIONS

Galaxies for this study were selected from the HI Parkes All-Sky Survey (HIPASS) Bright Galaxy Catalogue (BGC). HIPASS is a blind survey for HI covering the entire southern sky. The data reduction is described by Barnes et al. (2001). The 3σ HI mass limit of HIPASS is $\sim 10^6 D_{\text{Mpc}}^2 M_{\odot}$, the 3σ HI column density limit is $4 \times 10^{18} \text{ cm}^{-2}$ and the FWHM beamwidth is $15.5'$. The BGC is the largest blind HI extragalactic catalogue to-date. The galaxy finding and parameterisation is described by Koribalski et al. (2002). The HI masses in the BGC were calculated using Local Group corrected velocities and an $H_0 = 75 \text{ km s}^{-1} \text{ Mpc}^{-1}$.

HIPASS poorly resolves most galaxies and can usually only measure a lower limit to the column density, equivalent to the HI being smoothly spread over the entire beam. To measure the distribution of HI column densities, higher resolution mapping is required. Thirty-five galaxies were chosen at random from the BGC for mapping with the Australia Telescope Compact Array (ATCA)¹. To provide a representative range of HI mass, galaxies were chosen with an even mass distribution in the range $7.5 < \log M_{\text{HI}} < 10.5 M_{\odot}$. Galaxies were restricted to those with heliocentric velocities in the range 500 to 1700 km s^{-1} so that the spatial resolution remained comparable across the sample.

Each galaxy was observed with the ATCA 375 and 750D array configurations. The data set was reduced in MIRIAD, the velocity resolution in each datacube is 3.3 km s^{-1} . The datacubes have an average restored beam of $1' \times 1'$ and typical RMS noise in line-free regions of $3.7 \text{ mJy beam}^{-1}$, this

¹ The Australia Telescope Compact Array is part of the Australia Telescope which is funded by the Commonwealth of Australia for operation as a National Facility managed by CSIRO.

corresponds to a 3σ column density limit, over 3 velocity channels, of $2 \times 10^{19} \text{ cm}^{-2}$. The HI column density (N_{HI}) of each pixel in each galaxy was calculated by summing flux density along the spectral axis. The integrated flux density, Sdv (Jy km s^{-1}), was converted to a brightness temperature in the usual manner, $T_b = 1.36 \times 10^3 \lambda^2 S/b_{\text{maj}}b_{\text{min}}$, where λ is in cm and the major and minor beam axes, b_{maj} and b_{min} , in arcsec. T_b is converted to column density using $N_{\text{HI}} = 1.823 \times 10^{18} \int T_b dv \text{ cm}^{-2}$. This calculation assumes that the gas is optically thin. Dickey & Lockman (1990) used typical Galactic HI parameters ($T_s \sim 50\text{K}$ and $\Delta v \sim 10\text{km s}^{-1}$) to show that the optical depth is greater than 1 for $N_{\text{HI}} > 10^{21} \text{ cm}^{-2}$. Consequently the column density may be underestimated as N_{HI} approaches 10^{21} cm^{-2} , providing an upper limit to these observations. Regions of high N_{HI} may also be underestimated due to the resolution of the observations. Nearby galaxies which have been mapped at high resolution show many regions with $N_{\text{HI}} > 10^{21} \text{ cm}^{-2}$ (e.g. the LMC, Staveley-Smith et al. 2003). Table A1 summarises the HI parameters for each of these galaxies. Also included are optical parameters from the Lyon-Meudon Extragalactic Database (LEDA). Some galaxies are new or recent discoveries and therefore some optical parameters are unavailable. For example, HIPASS J0949-56 lies behind the Milky Way and no optical counterpart is visible due to high foreground extinction ($A_B=9.2$). Figure A1 gives the N_{HI} contours overlaid on a DSS image of each galaxy. An N_{HI} histogram for each galaxy is given in Figure A2.

3 DATA ANALYSIS

The column density distribution function, from each galaxy (i) in the sample, is calculated using

$$f(N_{\text{HI}}) = \frac{c}{H_0} \frac{1}{N} \sum_{i=1}^N \frac{\phi(M_{\text{HI}})_i A(N_{\text{HI}})_i}{dN_{\text{HI}}} \quad [\text{cm}^2], \quad (1)$$

where $A(N_{\text{HI}})$ is the area in Mpc^2 occupied by column densities in the range N_{HI} to $N_{\text{HI}} + dN_{\text{HI}}$ ($d \log N_{\text{HI}} = 0.2$ dex is used throughout). The function is normalised by the space density, $\phi(M_{\text{HI}})$ taken from the HIPASS BGC HI mass function (Zwaan et al. 2003), which has a faint end slope of $\alpha = -1.30 \pm 0.08$ and a characteristic HI mass of $\log(M^*/M_\odot) = 9.79 \pm 0.06$ and normalisation $\theta^* = (8.6 \pm 2.1) \times 10^{-3} \text{ Mpc}^{-3}$. The resulting distribution function is plotted in Figure 1. A power law, $f(N_{\text{HI}}) = BN_{\text{HI}}^{-\beta}$, is fitted with $\beta = 1.5 \pm 0.1$ in the range $19.6 < \log N_{\text{HI}} < 21.6$. The three highest column density points do not agree well with this power law. A double power law is therefore fitted with a break at $\log N_{\text{HI}} = 20.9$. In this case the lower column densities, $19.6 < \log N_{\text{HI}} < 20.9$, are best fitted with $\beta = 1.4 \pm 0.2$ and the upper column densities, $20.9 < \log N_{\text{HI}} < 21.6$, with $\beta = 2.1 \pm 0.9$. The double power law is also given in Figure 1.

The $z = 0$ $f(N_{\text{HI}})$ from 21-cm is compared to higher redshift measurements from QSO absorption line studies. The high redshift ($\langle z \rangle \sim 2.5$) DLA measurements are taken from Storrie-Lombardi & Wolfe (2000) and the intermediate redshift ($\langle z \rangle \sim 0.78$) DLA measurements from Rao & Turnshek (2000). (Although q_0 is unimportant at

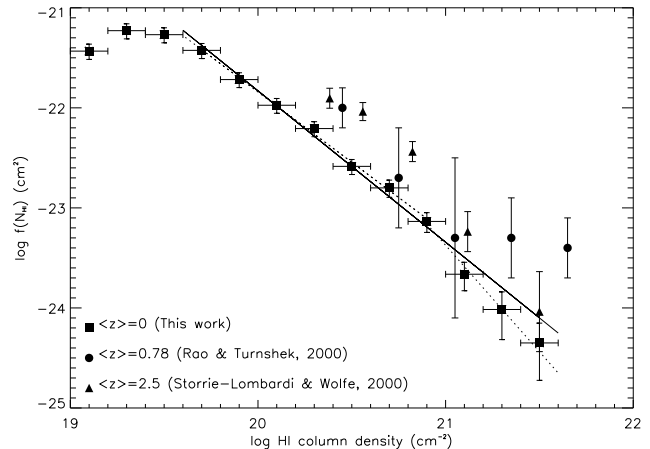


Figure 1. Column density distribution function at $z = 0$ for all galaxies in the sample (data points). The error bars are calculated using Poisson statistics. A comparison is made to the high redshift ($\langle z \rangle = 2.5$) measurements of Storrie-Lombardi & Wolfe (2000) (triangles) and intermediate redshift ($\langle z \rangle = 0.78$) measurements of Rao & Turnshek (2000) (circles). The distribution is fitted with a single power law (solid line) and double power law (dotted line).

$z = 0$, the high redshift $f(N_{\text{HI}})$ and dN_{DLA}/dz use $q_0 = 0$.) We find that with decreasing redshift, $f(N_{\text{HI}})$ decreases at all column densities and flattens for $20.9 < \log N_{\text{HI}} < 21.6$ from $\langle z \rangle \sim 2.5$ to 0. Quantitatively, the flattening is determined by fitting a power law in this high N_{HI} range to the $\langle z \rangle \sim 2.5$ ($\beta = 2.5$) and $z = 0$ ($\beta = 2.1$) distribution functions. The flattening of $f(N_{\text{HI}})$ at high column densities is attributed to growth of denser objects (i.e. galaxies), therefore reducing the number of lower column density systems and increasing the high N_{HI} systems. The overall decrease in $f(N_{\text{HI}})$ to $z = 0$ can be explained by the consumption of HI gas to form stars. The magnitude of the Rao & Turnshek (2000) $f(N_{\text{HI}})$ fits with the general evolutionary picture. However the slope of the function is not in good agreement, although the error bars are large enough for the above description to hold within the stated uncertainties.

The departure from the power law at $N_{\text{HI}} < 10^{20} \text{ cm}^{-2}$ is perhaps partly due to the HI-HII transition, described as the “footprint” of ionisation by Corbelli et al. (2001), essentially marking the HI edge of the galaxies. It may also be due to the detection limit of our observations. The detection limit is a function of the line width, so measurements of low column density regions of galaxies with large line widths are most likely underestimated.

Systematic uncertainties in $f(N_{\text{HI}})$ could arise from errors in the galaxy distances or the HI mass function. The distance to each galaxy was calculated using the radial velocity, corrected for the motion of the Local Group. Alternatively, a parametric model for the velocity field of galaxies can be used to calculate distance. The model used is by Tonry et al. (2000), uncertainties in the distance affects the $\phi(M_{\text{HI}})$ and $A(N_{\text{HI}})$ terms in $f(N_{\text{HI}})$. The difference between the two distance calculations is $\sim 20\%$ for most galaxies in the sample. The resulting $f(N_{\text{HI}})$ is plotted in Figure 2 along with the original calculation. In addition, $f(N_{\text{HI}})$ is calculated with two different HI Mass functions, one with shallower slope (Zwaan et al. 1997) and one with a

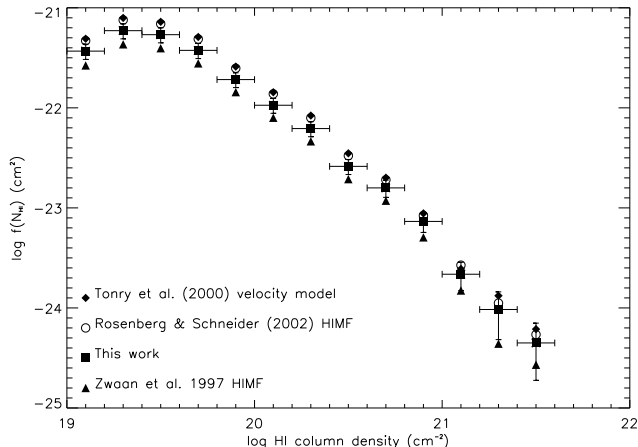


Figure 2. The effect of systematic errors on the column density distribution function. The original function is included along with two different HI mass functions (Zwaan et al. 1997; Rosenberg & Schneider 2002) and a velocity flow model to calculate the distance to each galaxy (Tonry et al. 2000). The different functions show that systematic uncertainties are small and have little effect on the shape of $f(N_{\text{HI}})$.

stepper slope (Rosenberg & Schneider 2002). These systematic uncertainties have little effect on the shape and normalisation of the column density distribution function beyond the random errors already quoted.

The power law slope of the column density distribution is theoretically predicted to be -3 at the high N_{HI} end for disc galaxies (Milgrom 1988; Wolfe et al. 1995). This prediction together with a measured $f(N_{\text{HI}})$ slope flatter than -3 has been used to argue that disc galaxies cannot be responsible for all DLA systems (Rao & Turnshek 2000). Considering only the spiral galaxies in the sample, we find that $f(N_{\text{HI}})$, for $N_{\text{HI}} \geq 10^{21} \text{ cm}^{-2}$, has a power law slope of -2.6 ± 1.0 . In Figure 3, $f(N_{\text{HI}})$ for each spiral galaxy contributing to this N_{HI} range is shown. If we consider both spiral and non-spiral galaxy types, the power law slope in this high N_{HI} region increases to -2.1 ± 0.9 . Thus, including non-spiral galaxies in the sample, the data still agrees, within the uncertainties, with the theoretical prediction for spiral galaxies only.

To emphasise the relationship between $f(N_{\text{HI}})$ and total galaxy HI mass these are plotted in a range of column density bins in Figure 4. $f(N_{\text{HI}}, M_{\text{HI}})$ has the same basic shape at all column densities. For most N_{HI} , $f(N_{\text{HI}}, M_{\text{HI}})$ is essentially a flat function of HI mass, rising slightly from $\log M_{\text{HI}} = 9$ to $9.5 M_{\odot}$ and dropping off sharply after $\log M_{\text{HI}} = 10 M_{\odot}$. To compare with DLA absorption line statistics, we also integrate $f(N_{\text{HI}})$ from $N_{\text{HI}} \geq 2 \times 10^{20} \text{ cm}^{-2}$, which is equivalent to calculating the cross-section of HI satisfying the DLA criteria, or the number density of DLAs per unit redshift.

$$\frac{dN_{\text{DLA}}}{dz} = \int_{N_{\text{HI}}=2 \times 10^{20}}^{N_{\text{HI,max}}} f(N_{\text{HI}}) dN_{\text{HI}} \quad (2)$$

For the whole sample, $dN_{\text{DLA}}/dz = 0.058 \pm 0.006$ (random) $^{+0.03}_{-0.02}$ (systematic) at $z = 0$. The random uncertainty is based on Poisson statistics and the systematic uncertainty

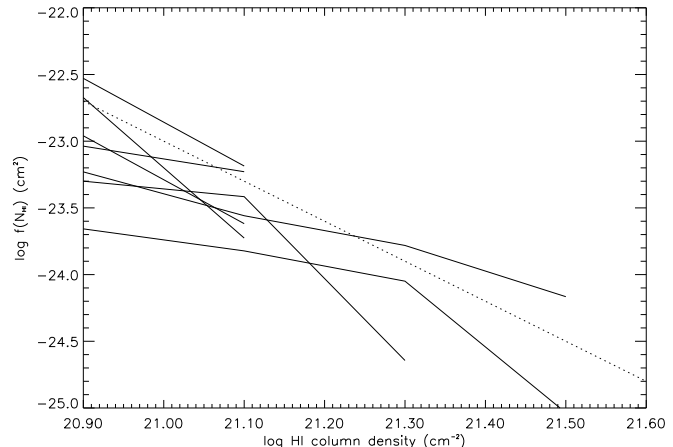


Figure 3. Column density distribution function for individual spiral galaxies only (solid lines). The dotted line, N_{HI}^{-3} , is predicted theoretically (arbitrary normalisation).

is from the HI mass function. This value agrees very well with the parameterisation, $dN_{\text{DLA}}/dz = 0.055(1+z)^{1.11}$ over a large redshift range by Storrie-Lombardi & Wolfe (2000) (see their Figure 11). This result confirms the suggestion by Storrie-Lombardi & Wolfe (2000) that there is no intrinsic evolution in the product of space density and cross-section of DLAs with redshift to $z = 0$.

Figure 5 compares the fractional contribution of dN_{DLA}/dz to the HI mass density, $\rho_{\text{HI}} = \phi(M_{\text{HI}}) \times M_{\text{HI}}$ as a function of $\log M_{\text{HI}}$. The histogram shows that 34% of dN_{DLA}/dz can be attributed to galaxies with $\log M_{\text{HI}} < 9.0$. This is in contrast to ρ_{HI} (continuous line in figure), which is dominated by M^* galaxies. In comparison 26% of ρ_{HI} is due to galaxies with $\log M_{\text{HI}} < 9.0$. Furthermore, Figure 6 shows that the mean DLA cross-section of $\log M_{\text{HI}} < 9.0$ galaxies is a mere 4%.

Although the cross-section of HI satisfying the DLA criterion in an individual low HI mass galaxy may be small, the product of cross section and space density is more significant than the product of HI mass and space density. This leads to dN_{DLA}/dz as a function of HI mass peaking at less than M_* . Low mass galaxies may contribute little to the HI mass density, however they make up an important part of dN_{DLA}/dz .

This result is similar to Rosenberg & Schneider (2003) if the different HI mass functions are considered. In both cases the dN_{DLA}/dz histogram generally sits slightly above ρ_{HI} for $M_{\text{HI}} < M^*$ and slightly below for $M_{\text{HI}} > M^*$. Rosenberg & Schneider (2003) find a tight correlation between $\log M_{\text{HI}}$ and $\log A(N_{\text{HI}} \geq 2 \times 10^{20} \text{ cm}^{-2})$ and use this to calculate dN_{DLA}/dz . In that case $\rho_{\text{HI}} \propto dN_{\text{DLA}}/dz$, so the shape of $\rho_{\text{HI}}(M_{\text{HI}})$ should match $dN_{\text{DLA}}/dz(M_{\text{HI}})$ peaking at M^* . In practice the shape of dN_{DLA}/dz deviates slightly from ρ_{HI} since Rosenberg & Schneider (2003) use the $1/V_{\text{tot}}$ value for each individual galaxy rather than $\phi(M_{\text{HI}})$ from the function form of the HI mass function.

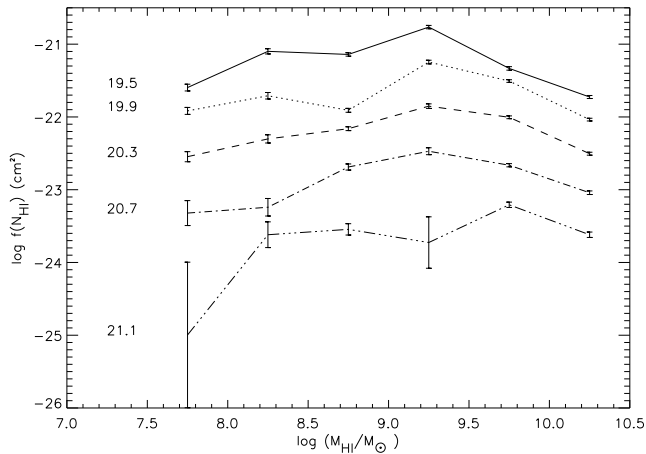


Figure 4. Column density distribution function at $z = 0$ as a function of galaxy HI mass, plotted at six different column densities.

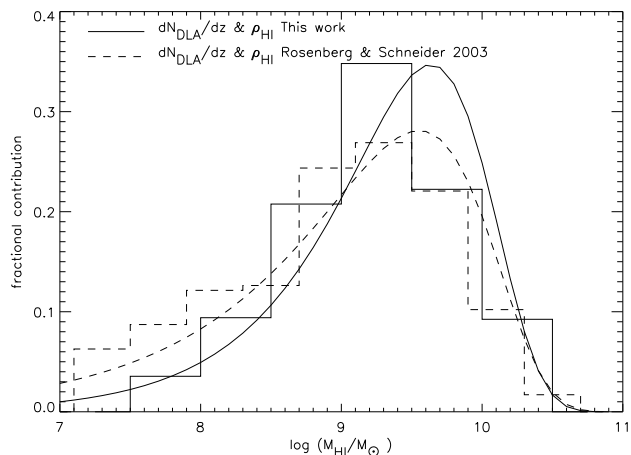


Figure 5. Fractional contribution of each HI mass bin to dN_{DLA}/dz (histogram) and HI mass density, ρ_{HI} ($M_{\odot} Mpc^{-3}$, continuous line) comparing the work in this paper (solid histogram and line) with Rosenberg & Schneider (2003) (dashed histogram and line).

3.1 Relationship between DLA-gas and Optical Properties

In this section we explore the relationship between dN_{DLA}/dz and optical properties of galaxies in the sample. dN_{DLA}/dz is still normalised by the HI mass function, but is weighted to reflect the number distribution of optical properties in the sample. The mean DLA cross-section, $A(N_{HI} \geq 2 \times 10^{20} cm^{-2})$, for galaxies with each different property is also calculated. The fractional contributions to dN_{DLA}/dz and mean DLA cross-section as a function of each galaxy property is given in Figures 7 to 10. In each case the dN_{DLA}/dz contribution (solid histogram) describes the probability of a galaxy with a particular property giving rise to a DLA system. The mean DLA cross-section (dashed histogram) indicates for a galaxy with a particular property, its non-weighted DLA cross-section on the sky.

First, the likelihood of a galaxy in different luminosity

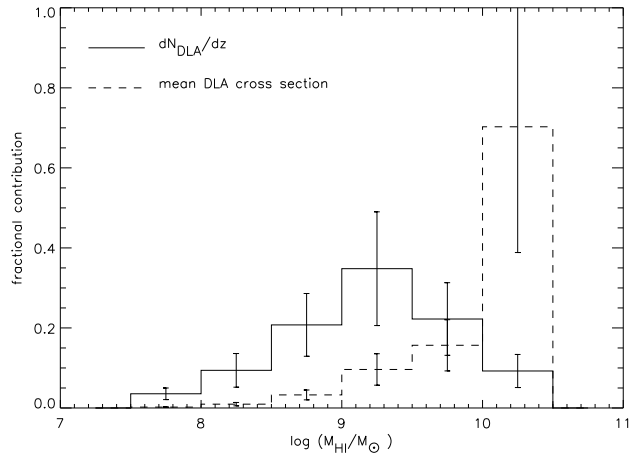


Figure 6. Fractional contribution of each HI mass bin to dN_{DLA}/dz (solid line) and the mean DLA cross-section (dashed line).

ranges giving rise to a DLA system is calculated. Galaxies in the range $8 L_{\odot} < \log L_B < 10 L_{\odot}$ dominate dN_{DLA}/dz . Sub- L_* ($\log L_B < 9 L_{\odot}$) galaxies account for 45% of the DLA cross-section. In contrast these sub- L_* galaxies have very small (6%) DLA cross-sections compared with $L > L_*$ galaxies. This has interesting consequences for the interpretation of DLA-galaxy associations. For example, although sub- L_* galaxies are just as likely to give rise to a DLA absorber, given a DLA system in a field with one sub- L_* and one super- L_* galaxy, the super- L_* galaxy is ~ 10 times more likely to be responsible for the DLA by virtue of its much larger HI cross-section.

To investigate the relationship between dN_{DLA}/dz and galaxy morphology, the sample was divided into three parts. The first group contains Irregular and Magellanic-type galaxies. The second group, late type spirals, includes Sd and Sc types. The early type spiral group is comprised of Sb, Sa and S0 types. We find that dN_{DLA}/dz is dominated by late type spirals, which contribute 48% to the cross-section of DLA-gas on the sky. The contribution of Irregular and Magellanic types is non-negligible at 25%. Individually however, early type spirals each have the largest DLA cross-section (40%).

dN_{DLA}/dz as a function of galaxy mean surface brightness within the magnitude 25 isophote ($\bar{\mu}_{25}$) is dominated by galaxies with $23 < \bar{\mu}_{25} < 24$ mag arcsec $^{-2}$. The mean DLA cross-section of these galaxies also dominate the surface brightness division. Lower surface brightness galaxies, with $\bar{\mu}_{25} > 24$ mag arcsec $^{-2}$, make up 22% of the cross-section. Five galaxies did not have this parameter available in the LEDA database. One of these is HIPASS J0949-56, which lies behind the Milky Way. Another, HIPASS J1320-21 is a high surface brightness S0 galaxy. The other three (HIPASS J0905-56, J1321-31 and J2222-48) all appear to be LSB galaxies (see Figure A1). The fact that these galaxies are missing from the analysis introduces a bias against low surface brightness galaxies. Including these three galaxies in the lowest surface brightness bin ($25 < \bar{\mu}_{25} < 26$ mag arcsec $^{-2}$) increases the dN_{DLA}/dz contribution from 3 to $6 \pm 5\%$.

The relationship between dN_{DLA}/dz , HI mass and L_B

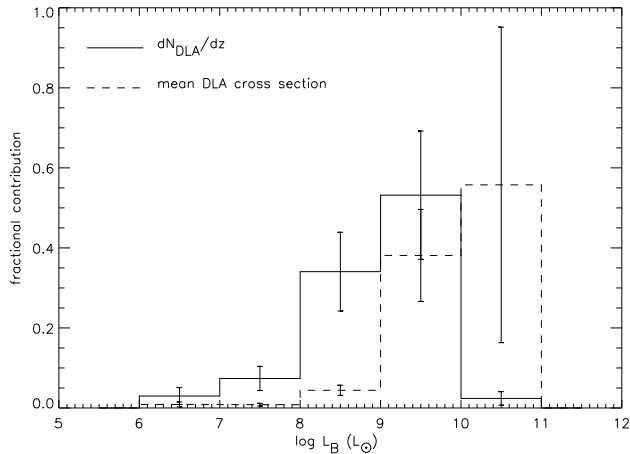


Figure 7. Fractional contribution of each luminosity decade to dN_{DLA}/dz (solid line) and the mean DLA cross-section (dashed line).

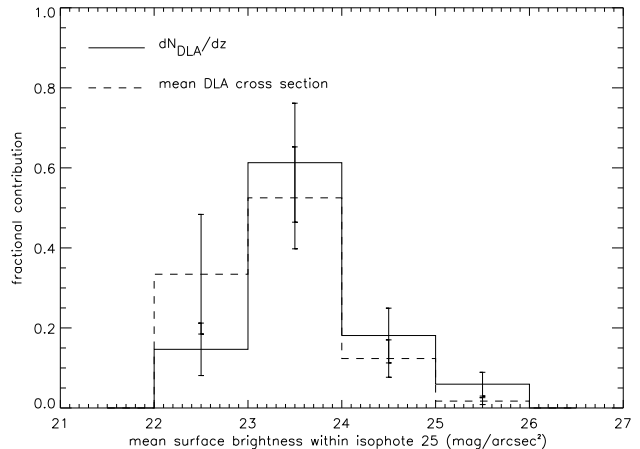


Figure 9. Fractional contribution of each mean surface brightness decade to dN_{DLA}/dz (solid line) and the mean DLA cross-section (dashed line).

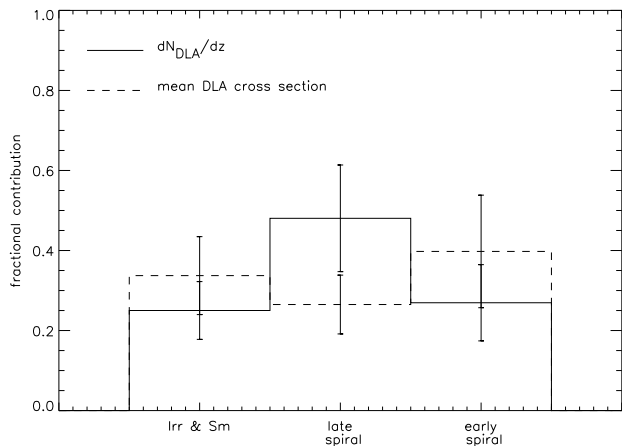


Figure 8. Fractional contribution of each morphological type to dN_{DLA}/dz (solid line) and the mean DLA cross-section (dashed line).

is combined in the calculation of $M_{\text{HI-to-}L_B}$ ratio. The cross section of DLA-gas is dominated by gas-rich galaxies with $M_{\text{HI-to-}L_B}$ ratios in the range 1 – 10. The very high $M_{\text{HI-to-}L_B}$ ratio galaxies contribute little to the DLA cross section (5%), mostly due to their rarity. It is also due to the fact that most of the HI in these galaxies has a low column density. The contribution of very high $M_{\text{HI-to-}L_B}$ ratio galaxies to dN/dz for $\log N_{\text{HI}} \leq 19.1 \text{ cm}^{-2}$ is $18 \pm 5\%$.

4 DISCUSSION

The flattening of $f(N_{\text{HI}})$ between $\langle z \rangle = 2.5$ and $z = 0$ for $N_{\text{HI}} \gtrsim 10^{20.5} \text{ cm}^{-2}$ can be explained by accreting clumps of HI into the central regions of galaxies and DLA systems. Milgrom (1988) argues that the slope of the column density distribution function reflects the density distribution within the absorbers themselves. A case is presented where lines of sight through spherical gas clouds give rise to $f(N_{\text{HI}}) \propto N_{\text{HI}}^{-\beta}$. The column density profile of each sphere

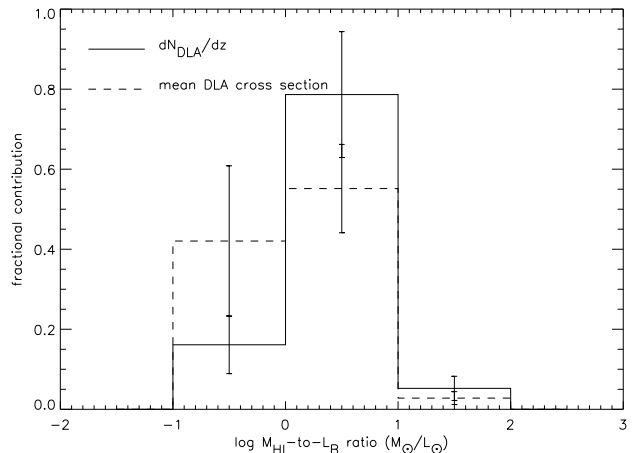


Figure 10. Fractional contribution of each mass-to-light ratio decade to dN_{DLA}/dz (solid line) and the mean DLA cross-section (dashed line).

is given by $N_{\text{HI}}(l) = N_o[1 + (l/r_c)^2]^{-c}$, where l is the impact parameter and r_c is the core radius. The power law indices of the local and global distribution are related through $\beta = (c + 1)/c$. The high redshift column density distribution (Storrie-Lombardi & Wolfe 2000), for $N_{\text{HI}} \geq 10^{20.5} \text{ cm}^{-2}$, has a power law index of $\beta = 2.2$. Comparing $\beta = 2.2$ (with $c = 0.8$) to our $z = 0$ measurement of $\beta = 1.6$ (with $c = 1.7$), yields a more centrally concentrated column density profile for galaxies (or DLAs) at $z = 0$. This picture lends support to the hierarchical construction of galaxies and DLAs. The alternative model, monolithic collapse into disc-like systems, predicts $f(N_{\text{HI}}) \propto N_{\text{HI}}^{-3}$ for very high column densities ($N_{\text{HI}} \geq 10^{21} \text{ cm}^{-2}$). Our data is marginally consistent with this theoretical prediction for disc galaxies. However, we are unable to confirm a shallower power law for non-disc galaxies, because of a lack of measured high column densities, due to resolution limitations.

The number density of DLA systems per unit redshift is calculated to be $dN_{DLA}/dz = 0.058 \pm 0.006$ (random) $^{+0.03}_{-0.02}$ (systematic) at $z = 0$. This result agrees well with

an extrapolation of higher redshift evolution measured by Storrie-Lombardi & Wolfe (2000). Our result is in moderate agreement (within the large uncertainties) with Churchill (2001) who finds $dN_{DLA}/dz = 0.08_{-0.05}^{+0.09}$ at $\langle z \rangle = 0.06$ from MgII QSO absorption systems. Our result is also consistent with the 21-cm studies by Zwaan et al. (2002) and Rosenberg & Schneider (2003) who find $dN_{DLA}/dz = 0.042 \pm 0.015$ and 0.053 ± 0.013 respectively.

The association of Ly α absorption lines with particular galaxies is a subject of much debate. Some statistical studies compare galaxy survey data complete to a limit of L_* with Ly α absorption systems (e.g. Penton et al. 2002). We have shown statistically, that sub- L_* galaxies account for 45% of the DLA cross-section at $z = 0$. If such a large proportion of galaxies are missed, the strength of the galaxy-absorber cross-correlation function may be underestimated.

The results presented here agree with the targeted searches for low redshift DLA galaxies that find a range of morphologies and luminosities. Unfortunately 21-cm emission measurements of galaxies are limited to $z < 0.1$, whereas the detection Ly α absorption is bounded only by the brightness of the background probe. However, we can project these results to redshifts beyond zero. We have shown that low HI mass, low luminosity galaxies contribute significantly to the DLA cross-section at $z = 0$. These types of galaxies are more common at higher redshifts (e.g. Ellis 1997). Provided the DLA cross-section of these types of galaxies do not get significantly smaller with redshift, it is likely they also account for an important part of the high redshift DLA cross-section.

In future studies, where the absorption-line statistics and properties of $z = 0$ DLA galaxies are better known, $f(N_{HI})$ and dN_{DLA}/dz from 21-cm emission will provide a test of possible biases in the DLA galaxy population. Selection effects include gravitational lensing of QSO-galaxy alignments, bringing otherwise dimmer QSOs into a statistical sample and creating a ‘by-pass’ effect where the line-of-sight avoids the galaxy centre (Smette et al. 1997). Although, Le Brun et al. (2000) showed that lensing is not important in the sample of DLA galaxies presented in Le Brun et al. (1997), they note that brighter QSOs may be affected. Spiral galaxies could be under-represented in the DLA galaxy population due to their large dust content, obscuring any background QSO (Ostriker & Heisler 1984). A recent study of radio loud QSOs (Ellison et al. 2001) found that a dust-induced bias in optical QSO surveys may have led to an underestimate of Ω_{DLA} and dN_{DLA}/dz by at most a factor of two. However, DLAs are 4 times as likely to be found in the proximity of radio loud QSOs (Ellison et al. 2002) which could overestimate Ω_{DLA} and dN_{DLA}/dz . If the DLA cross-section from both 21-cm and QSO absorption is well measured and compared these biases can be better understood.

5 CONCLUSIONS

We have calculated the column density distribution function at $z = 0$ from an HI-selected sample of galaxies. We find that $f(N_{HI})$ follows a power law with slope = -1.5 ± 0.1 in the range $19.6 < \log N_{HI} < 21.6$. When compared to high redshift QSO absorption line data, $f(N_{HI})$ flattens and

decreases with evolution to $z = 0$. This evolution can be interpreted as accretion of lower column density systems onto higher ones, thus reducing the number of low column density galaxies. This picture fits with the hierarchical formation model of galaxies and DLA systems. Conversely, we are in marginal agreement with the theoretical prediction $f(N_{HI}) \propto N_{HI}^{-3}$ for very high column densities in spiral discs. The fact that we find $f(N_{HI}) \propto N_{HI}^{-2.1 \pm 0.9}$ for very high column densities, for all types of galaxies, including spiral discs means that we cannot use this analysis to rule out the alternative model, that spiral discs are responsible for all DLA systems.

However, analyzing the the slope of the $f(N_{HI})$ power law is not the only method of determining the likely galaxy types which gives rise to DLA systems. The calculation of dN_{DLA}/dz as function of HI mass, luminosity, galaxy morphology, M_{HI} -to- L_B ratio and surface brightness reveals a range of galaxy types contribute to the cross-section of N_{HI} satisfying the DLA criteria. In particular we find that galaxies with $\log M_{HI} < 9.0$ make up 34% of dN_{DLA}/dz ; Irregular and Magellanic types contribute 25%; galaxies with surface brightness, $\bar{\mu}_{25} > 24$ mag arcsec $^{-2}$ account for 22% and sub- L_* galaxies contribute 45% to dN_{DLA}/dz . These results agree with findings from the imaging of low redshift DLA galaxies. Integrating over all galaxies in the sample we find that $dN_{DLA}/dz = 0.058$, which is consistent with no intrinsic evolution in the product of space density and cross-section of DLAs with redshift. This result agrees with the redshift evolution predicted from high and intermediate DLA systems (Storrie-Lombardi & Wolfe 2000) and is moderately consistent with very low redshift QSO absorption line studies (Churchill 2001).

REFERENCES

- Barnes D. G., et al., 2001, MNRAS, 322, 486
 Boissier S., Péroux C., Pettini M., 2002, MNRAS, accepted, astro-ph/0208457
 Bowen D. V., Huchtmeier W., Brinks E., Tripp T. M., Jenkins E. B., 2001, A&A, 372, 820
 Bowen D. V., Tripp T. M., Jenkins E. B., 2001, AJ, 121, 1456
 Chengalur J. N., Kanekar N., 2002, A&A, 388, 383
 Churchill C. W., 2001, ApJ, 560, 92
 Corbelli E., Salpeter E. E., Bandiera R., 2001, ApJ, 550, 26
 Dickey J. M., Lockman F. J., 1990, ARA&A, 28, 215
 Ellis R. S., 1997, ARA&A, 35, 389
 Ellison S. L., Yan L., Hook I. M., Pettini M., Wall J. V., Shaver P., 2001, A&A, 379, 393
 Ellison S. L., Yan L., Hook I. M., Pettini M., Wall J. V., Shaver P., 2002, A&A, 383, 91
 Haehnelt M. G., Steinmetz M., Rauch M., 1998, ApJ, 495, 647
 Jimenez R., Bowen D. V., Matteucci F., 1999, ApJ, 514, L83
 Koribalski B., et al., 2002, AJ, submitted
 Le Brun V., Bergeron J., Boisse P., Deharveng J. M., 1997, A&A, 321, 733
 Le Brun V., Smette A., Surdej J., Claeskens J.-F., 2000, A&A, 363, 837

- Milgrom M., 1988, *A&A*, 202, L9
- Miller E. D., Knezek P. M., Bregman J. N., 1999, *ApJ*, 510, L95
- Nestor D. B., Rao S. M., Turnshek D. A., Monier E., Lane W. M., Bergeron J., 2002, in *ASP Conf. Ser. 254: Extragalactic Gas at Low Redshift* p. 34
- Ostriker J. P., Heisler J., 1984, *ApJ*, 278, 1
- Penton S. V., Stocke J. T., Shull J. M., 2002, *ApJ*, 565, 720
- Pettini M., Ellison S. L., Steidel C. C., Shapley A. E., Bowen D. V., 2000, *ApJ*, 532, 65
- Prochaska J. X., Wolfe A. M., 1997, *ApJ*, 487, 73
- Rao S., Briggs F., 1993, *ApJ*, 419, 515
- Rao S. M., Turnshek D. A., 2000, *ApJS*, 130, 1
- Rosenberg J. L., Schneider S. E., 2002, *ApJ*, 567, 247
- Rosenberg J. L., Schneider S. E., 2003, *ApJ*, 585, 256
- Smette A., Claeskens J., Surdej J., 1997, *New Astronomy*, 2, 53
- Solanes J., Manrique A., García-Gómez C., González-Casado G., Giovanelli R., Haynes M. P., 2001, *ApJ*, 548, 97
- Staveley-Smith L., Kim S., Calabretta M. R., Haynes R. F., Kesteven M. J., 2003, *MNRAS*, 339, 87
- Storrie-Lombardi L. J., Wolfe A. M., 2000, *ApJ*, 543, 552
- Tonry J. L., Blakeslee J. P., Ajhar E. A., Dressler A., 2000, *ApJ*, 530, 625
- Turnshek D. A., Rao S., Nestor D., Lane W., Monier E., Bergeron J., Smette A., 2001, *ApJ*, 553, 288
- van Driel W., van Woerden H., Schwarz U. J., Gallagher J. S., 1988, *A&A*, 191, 201
- Wolfe A. M., Lanzetta K. M., Foltz C. B., Chaffee F. H., 1995, *ApJ*, 454, 698
- Wolfe A. M., Turnshek D. A., Smith H. E., Cohen R. D., 1986, *ApJS*, 61, 249
- Zwaan M., Briggs F. H., Verheijen M., 2002, in *ASP Conf. Ser. 254: Extragalactic Gas at Low Redshift* p. 169
- Zwaan M. A., Briggs F. H., Sprayberry D., Sorar E., 1997, *ApJ*, 490, 173
- Zwaan M. A., Verheijen M. A. W., Briggs F. H., 1999, *Publications of the Astronomical Society of Australia*, 16, 100
- Zwaan M., et al., 2003, *AJ*, accepted (astro-ph/0302440)

APPENDIX A: GALAXY SAMPLE

Includes a table of all the galaxies, an optical image with N_{HI} contours overlaid and a column density histogram for each galaxy.

This paper has been typeset from a $\text{\TeX}/\text{\LaTeX}$ file prepared by the author.

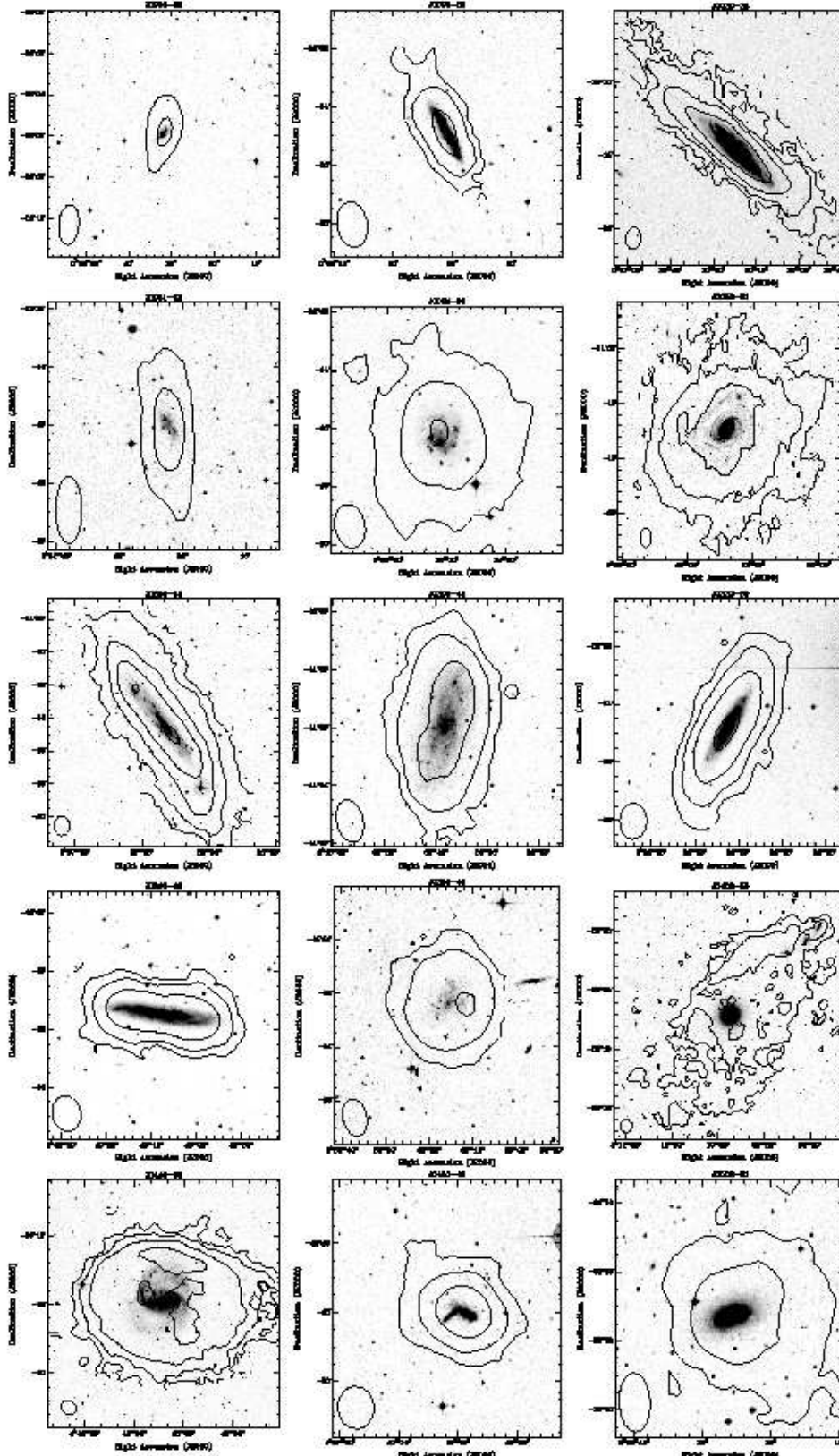


Figure A1. Optical images of galaxies in the sample with HI column density contours overlaid at $\log N_{\text{HI}} = 19.9, 20.3, 20.7, 21.1$ & 21.5 cm^{-2} . The restored beam is given in the bottom left-hand corner of each image.

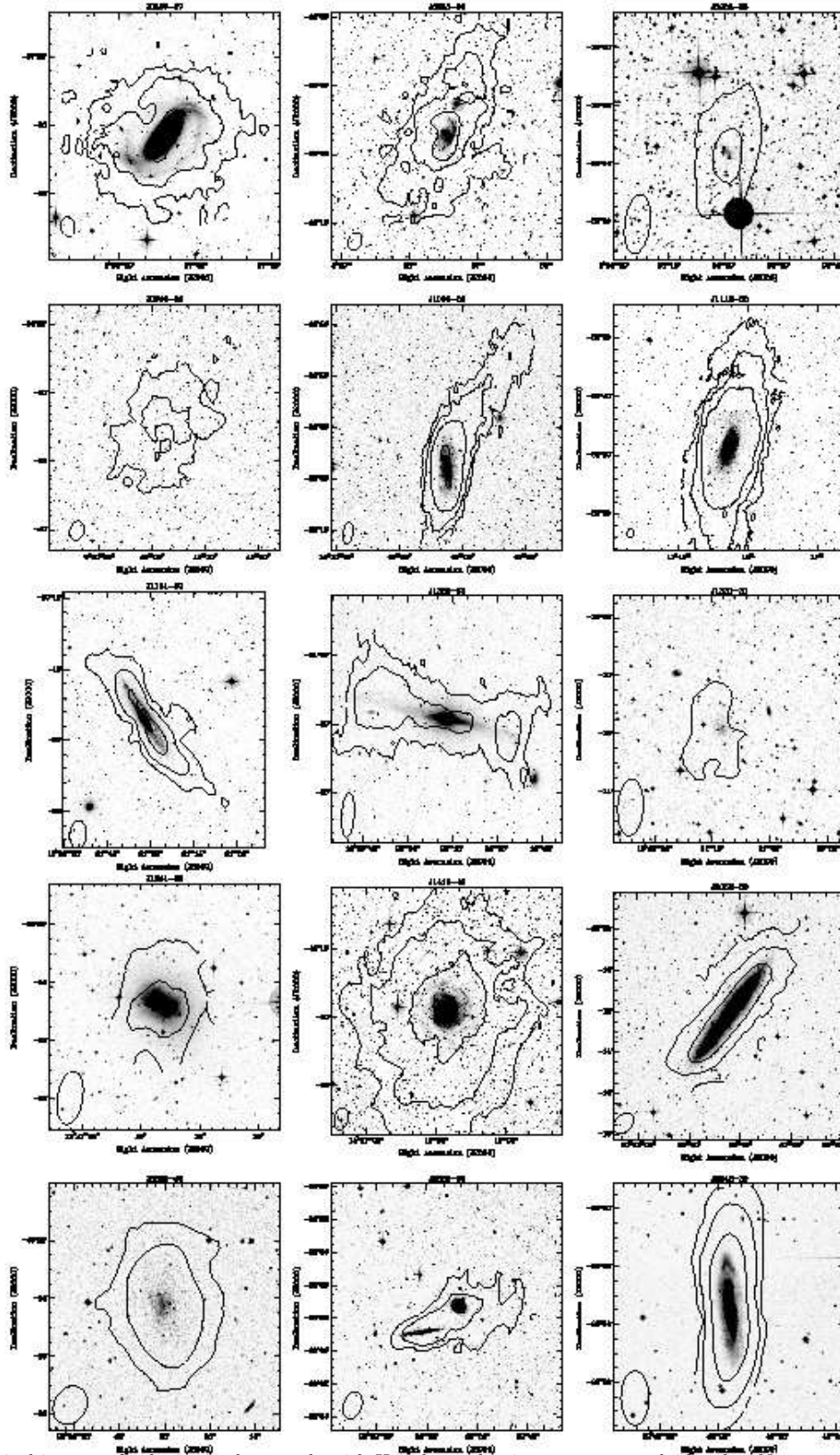


Figure A1 cont. Optical images of galaxies in the sample with HI column density contours overlaid at $\log N_{\text{HI}} = 19.9, 20.3, 20.7, 21.1$ & 21.5 cm^{-2} . The restored beam is given in the bottom left-hand corner of each image.

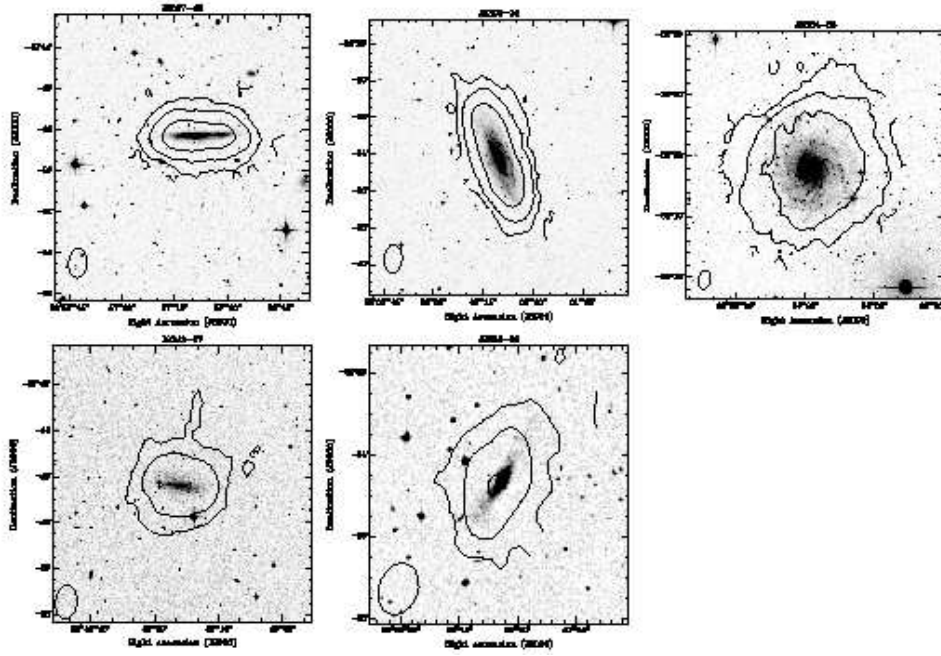


Figure A1 cont. Optical images of galaxies in the sample with HI column density contours overlaid at $\log N_{\text{HI}} = 19.9, 20.3, 20.7, 21.1$ & 21.5 cm^{-2} . The restored beam is given in the bottom left-hand corner of each image.

HIPASS Name	Optical ID	V_{hel} (km s ⁻¹)	Distance (Mpc)	log M_{HI} (M_{\odot})	beam (" × "(kpc))	$\bar{\mu}_{25}$ (mag " ⁻²)	M_{HI}/L_B (M_{\odot}/L_{\odot})	Morphology
J0005-28	ESO409-IG015	736	10.1	8.25	118×62(3.1)	24.0	2.2	Sc
J0008-29	NGC0007	1508	20.4	9.15	96×67(6.6)	23.7	2.2	SBc
J0030-33	NGC0134	1582	20.9	10.16	91×66(6.8)	23.5	1.3	SBbc
J0031-22	ESO473-G024	540	7.6	7.99	140×57(2.1)	24.1	5.4	Irr
J0034-30	UGCA006	1582	21.0	9.25	92×66(6.8)	24.0	2.9	SBm
J0052-31	NGC0289	1629	21.5	10.24	106×65(6.8)	23.9	2.5	SBbc
J0256-54	ESO154-G023	574	5.3	8.97	70×60(1.6)	24.0	6.8	SBm
J0309-41	ESO300-G014	955	10.8	8.86	90×58(3.1)	24.4	2.0	SBm
J0333-50	IC1959	640	6.1	8.37	74×60(1.8)	23.1	1.7	SBm
J0349-48	IC2000	981	10.5	8.92	75×62(3.2)	23.2	1.2	SBc
J0359-45	Horologium dwarf	898	9.5	8.60	86×57(2.6)	...	4.9	IB(s)
J0409-56	NGC1533	785	7.6	8.97	68×65(2.4)	22.8	0.9	S0
J0445-59	NGC1672	1331	14.6	10.00	75×59(4.3)	22.9	0.8	SBb
J0457-42	ESO252-IG001	657	5.9	7.95	74×67(1.9)	23.7	3.1	merger
J0506-31	NGC1800	809	8.1	8.28	103×57(2.3)	22.9	0.6	SBd
J0507-37	NGC1808	995	10.4	9.25	86×66(3.4)	23.3	0.4	SBa
J0857-69	ESO060-G019	1443	15.5	9.47	78×62(4.7)	23.3	1.9	SBcd
J0905-36	new	888	8.0	7.93	124×56(2.2)	Im
J0949-56	HIZSS059 ^a	1762	19.6	9.58	85×66(6.3)
J1009-29	NGC3137	1104	11.0	9.56	134×59(3.2)	23.9	2.6	SBc
J1118-32	NGC3621	730	6.2	9.91	95×79(2.4)	23.5	1.9	SBcd
J1131-30	NGC3717	1730	19.7	9.73	117×75(7.2)	23.9	1.4	Sb
J1320-21	NGC5084	1721	20.7	10.01	197×59(6.0)	...	1.2	S0
J1321-31	new ^b	571	5.0	7.54	119× 57(1.4)	...	11.2	Sm
J1341-29	NGC5264	478	4.0	7.68	112×56(1.1)	23.1	0.3	Irr
J1410-43	NGC5483	1771	21.1	10.09	102×63(6.4)	23.6	2.0	SBc
J2052-69	IC5052	584	5.9	8.93	71×50(1.4)	22.6	1.3	SBcd
J2222-48	ESO238-G005	706	8.9	8.47	85×70(3.0)	...	50.2	Irr
J2223-28	NGC7259	1780	24.5	9.56	104×70(8.4)	22.6	4.6	Sb
J2242-30	NGC7361	1249	17.3	9.47	113×62(5.2)	23.4	1.6	Sc
J2257-42	NGC7412A	930	12.1	8.79	86×59(3.5)	24.5	4.6	SBd
J2302-39	NGC7456	1199	15.9	9.42	91×62(4.8)	23.9	1.3	Sc
J2334-36	IC5332	701	9.3	9.51	97×60(2.7)	24.6	1.4	SBcd
J2349-37	ESO348-G009	648	8.4	8.35	90×59(2.5)	25.2	18.1	Irr
J2352-52	ESO149-G003	576	6.5	7.84	79×60(1.9)	23.9	1.8	Irr

Table A1. HI parameters for each galaxy from HIPASS and optical parameters from LEDA. The columns are the HIPASS name, optical ID, heliocentric velocity, distance (calculated using Local Group corrected velocities), HI mass, beam size of 21-cm map with the minor axis in kpc in parentheses, mean surface brightness within the 25th magnitude isophote, M_{HI} -to- L_B ratio and galaxy morphology.

^a Henning et al. (?)

^b Banks et al. (?)

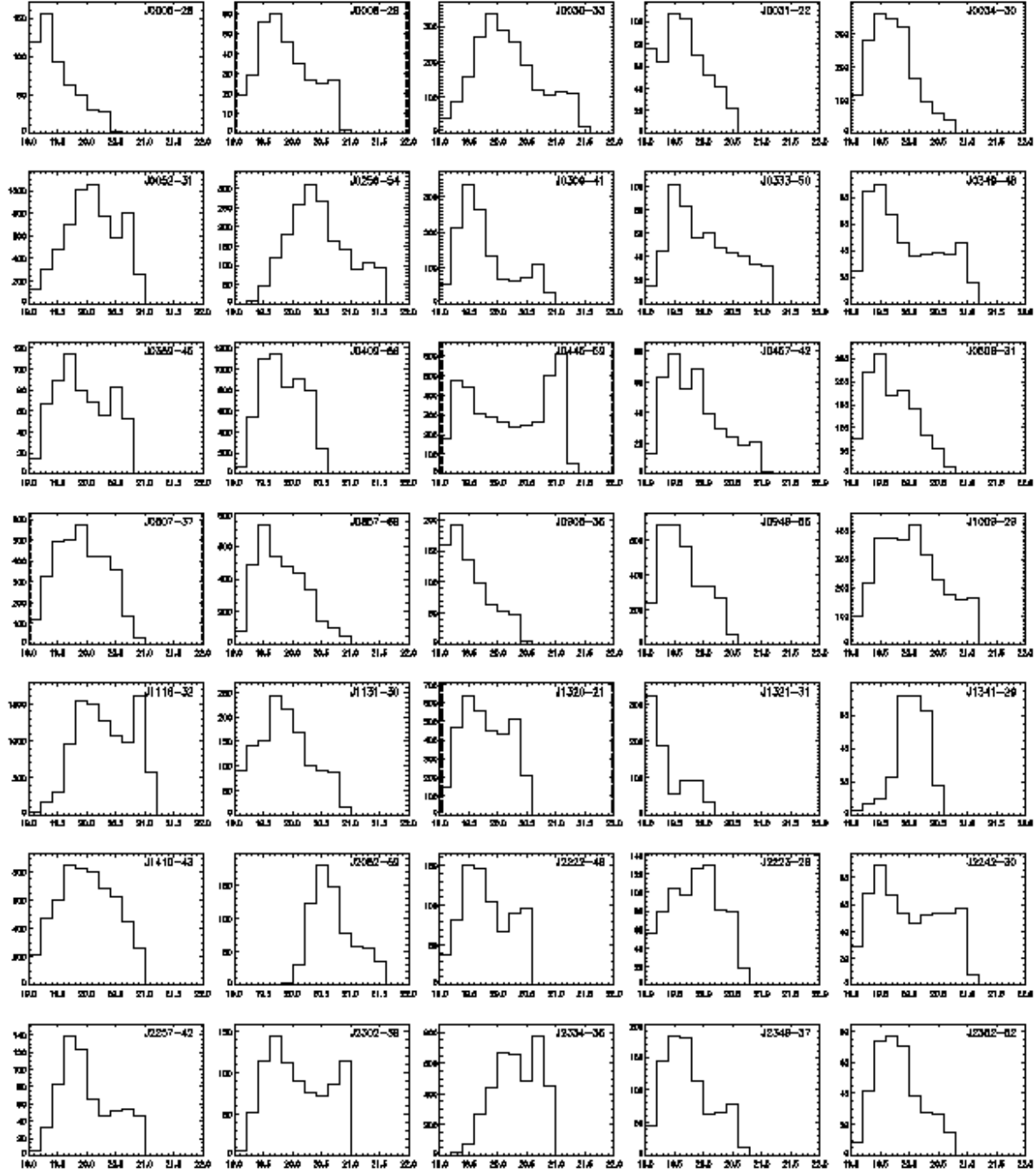


Figure A2. N_{HI} histograms for all galaxies in the sample. In each case, the x axis is $\log N_{\text{HI}} \text{ (cm}^{-2}\text{)}$ and the y axis is the number of pixels.